



The Genesis of the Epithermal Gold Mineralization at North Glojeh Veins, NW Iran.

Behzad Mehrabi^a, Majid Ghasemi Siani^{b*}, Hossein Azizi^c

^{a,b} *University of Kharazmi, Geosciences department, Tehran, Iran.*

^c *University of Kordestan, Engineering of Mining department, Sanandaj, Iran*

^b *E-mail address: majid4225@yahoo.com*

Abstract

The Glojeh mineralization district is part of Taron-Hashtjin metallogenic province. Igneous rocks in Glojeh district include intrusive rocks (granodiorite, granite and quartzmonzonite), and volcanic and sub-volcanic rocks (rhyodacite, rhyolite, andesitic basalt, andesitic, tachyandesite, trachydacite, basalt, tuff and rhyolitic tuff), which are typically of high-K igneous rocks transitional to shoshonites. Rhyodacite are host rocks of North Glojeh veins. Alteration is consisting of propylitization, sericitization, argillization and silicification. Hydrothermal alteration zones have well-developed and zoned, that extends \approx 30 meters into the host rocks. Mass balance calculations indicate that Al, Zr, Ti, Y, Nb, and HREE were immobile elements during alteration. Mineralization occur in four stages: 1) pyrite-magnetite-quartz assemblage; 2) As-Sb-Fe-Au-Cu assemblages; 3) Pb-Zn-Cu-Ag assemblages; and 4) hematite-goethite assemblages associated by precious metals. The veins longitudinal sections show clearly that base metals occur at the deepest levels, whereas precious metals occur at higher elevations with respect to base metals. Silver occur overlapping and slightly above the base metals zone, generally above the zone rich in base metals and beneath of gold zone. This observation contradicts the typical zoning pattern caused by boiling in epithermal veins. The North Glojeh deposit is a typical of epithermal deposit, with features of either high-sulfidation (stage 1 and 2) or intermediate-sulfidation (stage 3) types of epithermal deposits. Also stage 4 (oxidation zone) have features of low sulfidation type.

Keywords: Alteration; Epithermal; Mineralization; Genesis; Geochemistry

* Corresponding author.

E-mail address: majid4225@yahoo.com.

1. Introduction

Epithermal deposits form a spectrum with two end members; low and high sulfidation, that high sulfidation deposits are generally proximal with respect to the intrusion (probably porphyry deposits), whereas low sulfidation deposits occur generally distal [1]. Intermediate sulfidation deposits form part of the spectrum and their genesis is complex due to the involvement of fluids with meteoric or magmatic origin during their formation and due to fluid evolution. Epithermal-porphyry in world distributed in three main metallogenic provinces includes Circum Pasific, Alpine-Himalayan orogenic system and Paleo-Central Asian (Fig. 1) [2]. Subduction of the Paleo- and Neo-Tethys beneath the Eurasian and Iranian plates, respectively, caused the formation of the Caucasus magmatic arc in the north and the Sanandaj–Sirjan Magmatic Zone, the Urumieh-Dokhtar Zone, the Alborz Magmatic Belt, the Zagros fold-and-thrust belt in the south. Epithermal gold, base metal and porphyry deposits in Iran are mainly present in two magmatic belt along Paleo- and Neo-Tethys oceans includes Urmieh-Dokhtar (NW-trending) and Alborz (EW-trending) Magmatic Belt (Fig. 2), that are part of Alpine-Himalayan orogenic system [3, 4]. The Alborz Magmatic Belt is situated in northern Iran with an E-W orientation, and subdivided into eastern and western parts. Western portion merges with another Tertiary magmatic belt, the Urmieh-Dokhtar zone, which runs parallel to the main northwest-trending Zagros thrust [5, 6, 7]. Glojeh district is situated approximately 30 km (18.6 miles) north of the Zanjan town, and is located in Taron-Hashtjin metallogenic province (THMP). Structurally, THMP is located in merge between western Alborz Magmatic Belt and Urmieh- Dokhtar Zone (Fig. 2). The THMP have several mineralization of epithermal-porphyry and other type of ore deposits (Fig. 3). Glojeh district is one of the several epigenetic epithermal deposits in the THMP, and consists of a set of veins bearing polymetallic (Pb–Zn–Cu–Ag–Au) sulphides and recoverable amounts of Bi and Cd in North Glojeh and South Glojeh veins. This paper describes and reviews the principal geological characteristics, mineralization, alteration and geochemistry of epithermal gold deposits in North Glojeh.

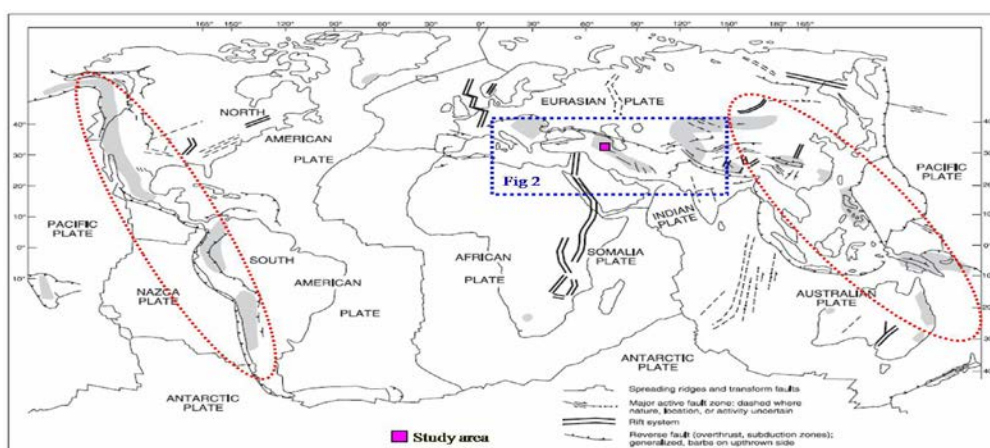


Fig. 1. Distribution of epithermal and porphyry provinces of the world [after 2], Circum Pasific (left), Alpine-Himalayan orogenic system (mid) and Paleo-Central Asian (right).

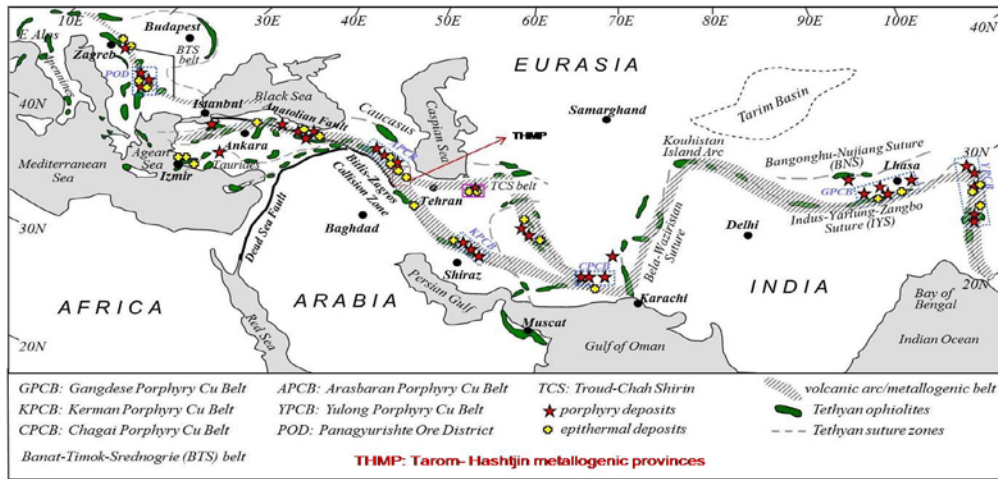


Fig. 2. Tethyan-Eurasian metallogenic belt [after 3, 4], epithermal-porphyry mineralization in Iran is part of Alpine-Himalayan orogenic system. Location of THMP show in figure (Fig. 3).

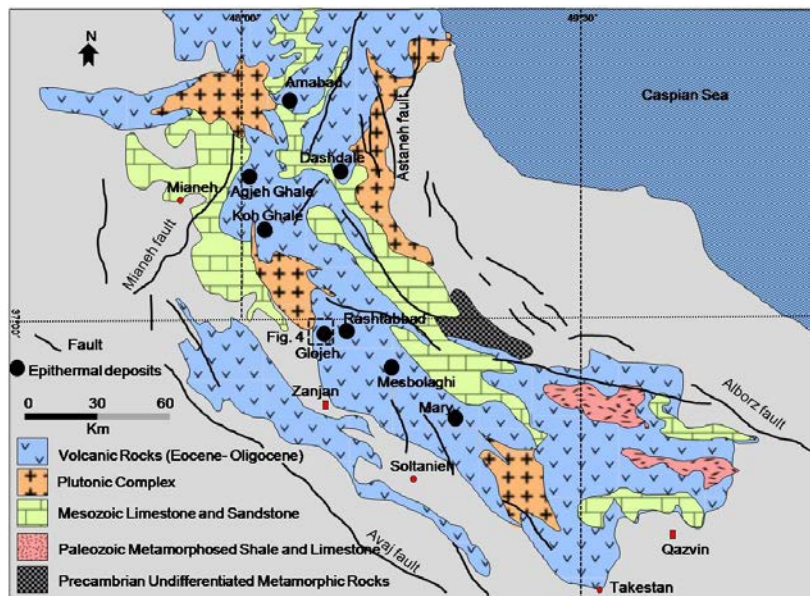


Fig. 3. Geological map of Tarom- Hashtjin metallogenic belt (THMP) and distribution of major epithermal ore deposits, Glojeh ore deposit located in mid of THMP.

2. Material and methods

Fifty six polished and thin-polished sections were studied by optical microscopy and FEI Quanta 650 FEG-ESEM and Zeiss 1450 vp SEM, at Leeds University and Iranian mineral processing research center (IMPRC), respectively. Electron microprobe analysis (EPMA) of polished and thin-polished sections carried out using Cameca SX100 at IMPRC. Operating conditions were: 20 kV and 20 nA, with a beam diameter 1-5 μm . Over 320 chemical assays from channel and drill core samples from North Glojeh veins were used in this study. The chemical analyses were performed in the chemistry laboratory of the Amdel Australia and Zarkavan Lab of Iran. Gold analyses are performed by fire assay and Ag, Pb, Zn, Cu, As, Sb are analyzed by inductively coupled plasma mass spectrometry (ICP-MS). Approximate detection limits for the elements are: Au=0.005 ppm, Ag=0.2 ppm, Pb, Zn and Cu=0.5

ppm. Interpolation of data and creation of longitudinal sections for the veins was done using the Kriging interpolation function built in the Surfer software, version 9. The basic statistics, minimum, maximum, mean and standard deviation were calculated for every vein by SPSS software, version 16.

3. Regional geology

The Glojeh ore mineralization is located in NW of Iran (Fig. 2), and is one of several epithermal ore deposits in THMP (Fig. 3). The THMP with 70 to 150 km width, 300 Km length and NW orientation hosts numbers of precious metals and polymetallic epithermal deposits associated with the Eocene to Oligocene volcano-plutonism. Regionally, the THMP comprises four tectonostratigraphic units (Fig. 3), namely: 1) Precambrian metamorphic basement, 2) Cambrian and Permian metamorphic rocks, 3) Jurassic to Cretaceous limestone and sandstone, and 4) Eocene to Oligocene volcano-plutonic rocks. Precambrian metamorphic rocks, are undifferentiated, and consist of schist, phyllite, and felsic rocks. Cambrian strata include dolomitic marble and phyllite, discordantly overlying the Precambrian metamorphic rocks. Permian low-grade metamorphic rocks discordantly overlies the Cambrian strata. The Permian strata, in turn, are discordantly overlain by Mesozoic rocks, consisting of, sandstone, limestone, and siltstone. The Cenozoic volcanic rocks, extensively distributed throughout the whole belt, comprise a wide spectrum of rock types, including trachybasalt, trachyandesite, andesite, andesitic-basalt, rhyodacite, rhyolite lava flows and tuff. Volcanic sequences in numerous places have been intruded by batholiths and smaller intrusions of granodiorite, quartzmonzonite and granite.

The major geological units of the Glojeh mineral district (Fig. 4) consist of three main lithologic units [8]. The first unit is characterized by pervasively well layered lithic tuff unit, and composed mostly of quartz phenocrysts, plagioclase and ubiquitous flattened fragments. The second unit is marked by basic tuff with interlayered andesitic basalt rocks. Basic tuffs and andesitic basalt volcanic rocks are exposed predominately in the southern district, whereas lithic tuffs are more abundant in northern part of the district. Andesitic basalts of dark yellow and brown are composed mostly of andesine and hornblende and biotite. Plagioclase occurs as phenocrysts. The third unit is rhyodacite unit, which only occur in the central and western segment of the Glojeh district (Fig. 4). Rhyodacites are characterized by phenocrysts of largely clay altered plagioclase, and smaller phenocrysts of variably altered feldspar, quartz and biotite, and various amounts of quartz, in a matrix rich in alkali feldspar. Several subvolcanic trachybasalt dykes characterized by quartz, biotite and plagioclase phenocrysts which intruded in lithic tuff unit. Two quartz monzonite, granite and granodiorite stock, located in the central (Goljin) and northern (Varmarziar) part of the district (Fig. 4), and younger rhyolite dome intrude in the rhyodacites volcanic section located in the west of district. The rhyolite domes are contains phenocrysts of plagioclase, quartz, and biotite. The intrusion comprises of plagioclase (30–45% by volume), quartz (25–30%), biotite (10–15%), alkali feldspar (8–10%), and hornblende (2%). Alkali feldspar with some perthitic exsolution was clearly a late phase to crystallise. Plagioclase is euhedral andesine. The N Glojeh veins are hosted along most of its length by the rhyodacite unit, except in its 100 m eastern extremity, where it enters in lithic and tuff unit.

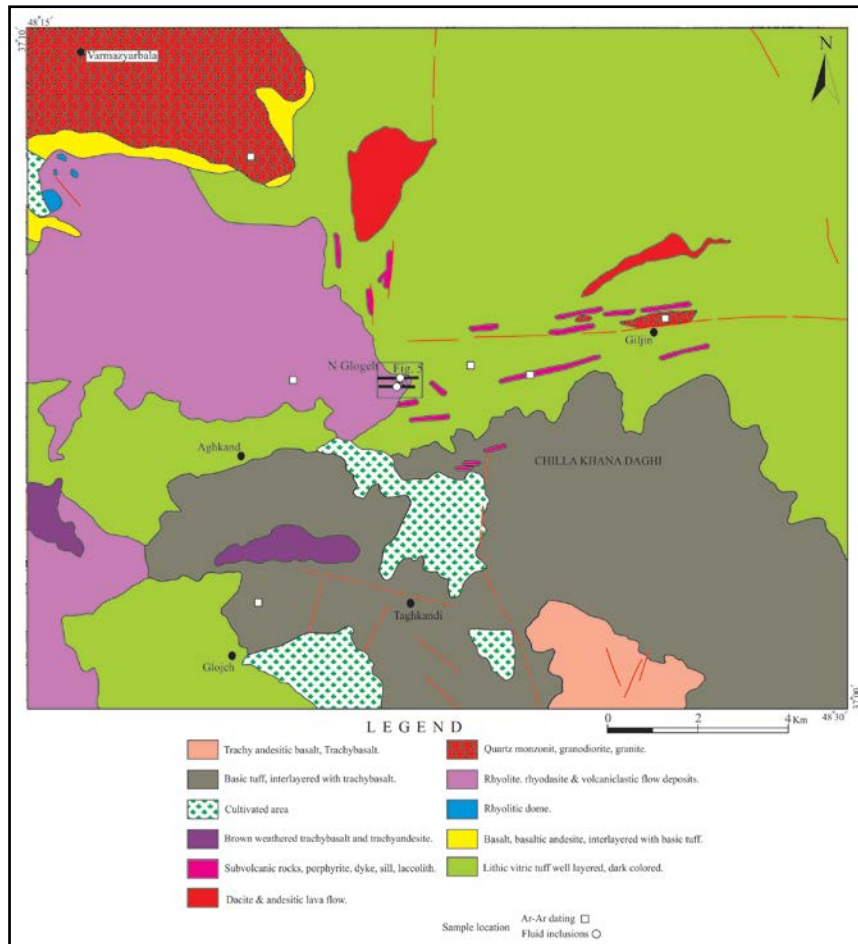


Fig. 4. Geological map of Glojeh area, (After 1/100000 geological map of Hashtjin [8] with revised).

4. Deposit geology

4.1. Host rocks and geological setting

Outcrops in the North Glojeh deposit from the oldest to youngest, comprises of; 1) lithic tuff with andesite interbedded; 2) rhyodacite with tuff interbedded, and; 3) lithic tuffs (Fig. 5). Mineralization in the North Glojeh deposit is mainly hosted by rhyodacite. Rhyodacite is widespread in east of district, and is black gray in altered surface and light gray in fresh surface (Fig. 6a). Several rhyolite dome intruded in rhyodacite unit (Fig. 6b). Rhyodacite consists predominantly of large phenocryst of altered plagioclase, feldspar and minor quartz in a fine-grained groundmass. Plagioclases are andesine and oligoclase, that replaced by kaolinite during alteration (Figs. 6c and 6d). Whole-rock major element analyses of 14 samples from volcanic and subvolcanic rocks were analyzed by Philips PW2404WD-XRF at the Kharazmi University in order to depict petrochemical characteristics and tectonic setting. The trace and rare earth elements analysis were carried out in the ACME laboratories, Vancouver, Canada (Table 1) using ICP-MS (Group 1T-MS) technique. According to the classification of [9], the volcanic rocks in Glojeh district fall into the fields of rhyodacite, rhyolite, andesitic basalt, andesitic, basalt, tuff and rhyolitic tuff (Fig. 7a). The rocks (Fig. 7b) are characterized by high K₂O contents (up

to 5.5 Wt. %), high average K₂O/Na₂O ratios (0.6), and high average Ce/Yb ratios (17.8), which are typical of high-K igneous rocks of transitional to shoshonitic series [10, 11].

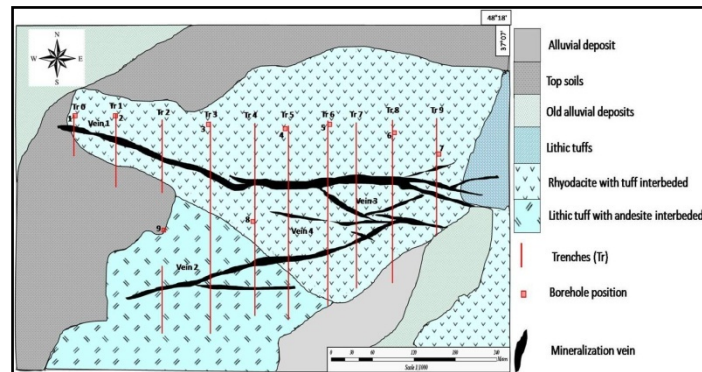


Fig. 5. Geological map of North Glojeh veins.

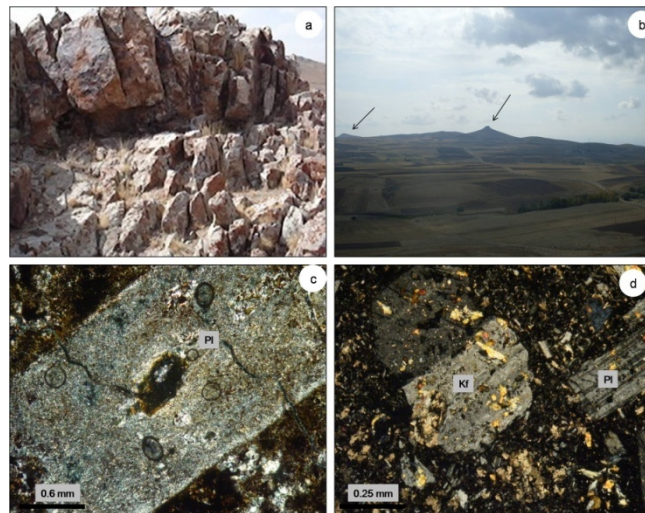


Fig. 6. Photographs and photomicrographs of representative rock types at North Glojeh, a) Rhyodacite rock that is host mineralization in North Glojeh, b) Rhyolite domes intrude in the rhyodacite volcanic section, c and d) K-feldspar and plagioclase phenocrysts replaced by kaolinite, calcite and chlorite. Abbreviations: Kf-K-feldspar, Pl-plagioclase.

4.2. Alteration and mass balance calculations

Hydrothermal alteration zones have well-developed and zoned around North Glojeh veins and extends \approx 30 meters into the host rocks, and are similar in both area. Laterally outward from the ore bodies, there are four alteration assemblages: (1) a silicic zone with massive and vuggy silica, and disseminated pyrite; (2) a low-intermediate intensity quartz-sericite-pyrite (QSP); (3) an argillic zones with quartz-kaolinite-montmorionite-illit-chlorite-pyrite and minor alunite; and (4) a propylitic zone consist of quartz-chlorite-calcite-epidote-sericite and albite.

Silicification is represented by the massive and vuggy silica bodies of crustiform quartz (Fig. 8b), anatase, Chalcedony and minor pyrite. Silicic alteration grades outward into sericite alteration, which is more widespread at depth. In the North Glojeh vein, the sericitic (QSP) alteration usually consists of

sericite (muscovite), quartz, and pyrite with minor calcite (Fig. 8f). These alteration products can be found as much as 5 m beneath the argillic zone, and more developed in depth rather than surface.

Argillic alteration (Fig. 8d) led to the crystallisation of quartz-kaolinite-montmorionite-illit-chlorite-pyrite and alunite and the bleaching of the wall rock. In general, argillisation is marked by the complete replacement of plagioclase and K-feldspar by these clay minerals. Argillic zone initiates with kaolinite-quartz and alunite (advanced argillic) (Fig. 8a), and is associated with sericite zone which host Cu-sulfide mierzalization, followed by montmorionite-illit and especially chlorite associated with base metals (stage 3B) (Fig. 8c). Propylitic alteration is the most widespread in the area and essentially consists of carbonate, epidote, chlorite, and albite (Fig. 8e). Propylitized rocks exist immediately adjacent to the veins where other alteration types are not present. Wherever other alteration assemblages are present, the propylitic assemblage is farther from the vein.

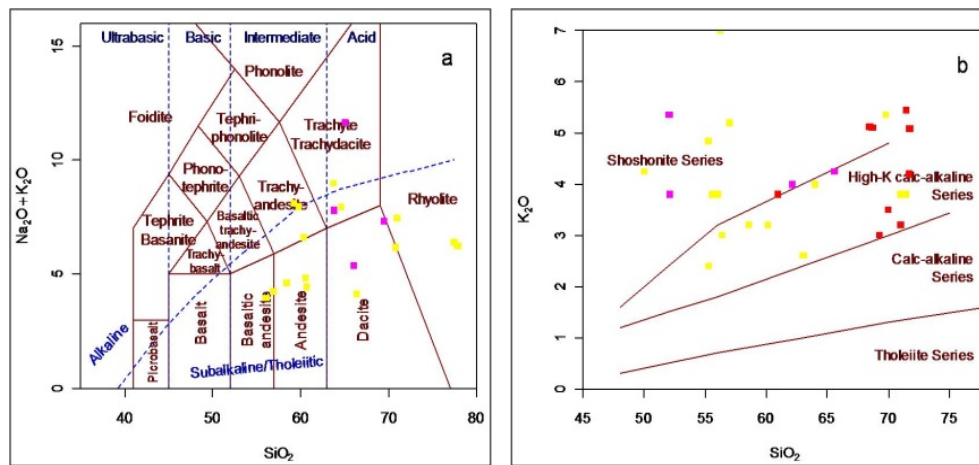


Fig. 7. Geochemistry of the volcanic and intrusion rocks. a) (Na₂O+K₂O) versus SiO₂, b) K₂O versus SiO₂ diagram . Yellow square (volcanic rocks), red square (intrusion rocks) and pink square (subvolcanic rocks).

The mass balance calculations were carried out using isocon method described by [12]. Twenty five sample of altered and fresh volcanic rocks analysis by ICP-MS and ICP-OES in Acme lab (Canada) and Kharazmi University, respectively. In this method the element mobility during alteration was quantified by plotting immobile elements (Al, Zr, Ti, Y, Nb, and HREE) in isocon plots. In argillic zone, HREE were immobile during alteration and plot close to a line of constant mass. Mass gains are apparent in Fe₂O₃, TiO₂, Th, Hf, As, Ni and V whereas mass losses in Na₂O, CaO, K₂O, MgO, Pb, Zn, Cu and Sb occur. In advanced argillic alteration, mass losses in REE, Nb, Pb, Sr, and Zr occur. This zone displays mass gains in Al₂O₃, As, Co, Ni, Hf and Nd. In sericitic (QSP) alteration, K₂O, Na₂O, MgO, CaO and LREE are enriched, whereas Fe₂O₃, and minor elements are depleted. In propylitic alteration, MgO and Al₂O₃ are enriched, whereas Fe₂O₃, K₂O, CaO, Na₂O, REE and minor elements are depleted (Fig. 9).

4.3. Mineralization and paragenetic sequence

There are two main veins (No. 1 and No. 2), and several veinlet, which strike E-W and generally dip steeply to the west in North Glojeh. The North Glojeh veins have length of greater than 1.5 km and a

width ranges from 0.1 to greater than 4 m (averages 2.5 m). Ore minerals textures are massive (up to 30 vol %), disseminated, replacement, banded (open space filling), and stockwork. Description and interpretation of cross-cutting relations between ore minerals were used to describe the vein stratigraphy. Mineralization at North Glojeh veins has been divided into four stages: Early stage (1) Pyrite-magnetite-quartz assemblage; Main stages (2) As-Sb-Fe-Cu-S assemblages; (3) Pb-Zn-Cu-Ag assemblages; and Late stage (4) Hematite-goethite-Ag-Bi-Au-Pb-S assemblages (Fig. 10).

Stage 1 is characterized by the deposition of vuggy and massive silica bodies contain massive to disseminated pyrite and magnetite. Pyrite occurs as euhedral and sometimes corroded and replaced by fine grained chalcopyrite, sphalerite and galena in later stages (Fig. 11a). Magnetite is anhedral and shows intergrowth with pyrite, and its composition is homogeneous. Stage 2 is characterized by the deposition of Cu-As-Sb-Fe-S assemblages as breccias and replacement bodies. Bornite associated with chalcocite occurs mostly as fracture fillings within chalcopyrite grains. In some places, it is present as subhedral to anhedral grains adjacent to chalcopyrite. Enargite associated with famatinite, chalcocite, covellit, bournonite and pyrite deposited around chalcopyrite (Fig. 11b). Hematite occurs as tabular shape, and contains gold grains (Fig. 11c), whereas sulfide minerals in this stage are without any trace of native gold. Pyrite is fractured and replaced by iron hydroxides, and in comparison with early stage pyrite, is enriched in arsenic (1.0 wt. %). The low-temperature polymorph of $Cu_3As_4S_4$, luzonite, has not been observed in veins. Medium grained quartz in associated with fluorite is the major gangue in stage 2. Stage 3 is subdivided into three sub-stages, and characterized by Pb-Zn (Cu±Ag) sulfides mineralization. Sub-stage 3A is characterized by the deposition of alternating veins, as symmetrical comb type texture, which initiated by deposition of coarse-grained quartz and fluorite, followed by coarse-grained sphalerite-galena and chalcopyrite deposited as intergrowth or inclusions mutually. Finally calcite, quartz and sericite deposited in center of veins bands. Sphalerite occurs mostly as subhedral to anhedral crystals adjacent to galena and chalcopyrite (Fig. 11d), and also as micro inclusions in galena and chalcopyrite crystals grains, and is characterized by green, white, honey yellow and brown internal reflections under crossed nicols. The iron content of sphalerite is generally low (0.4-1.0 wt. % and mean of 0.75wt. %), except in sphalerite with ‘‘chalcopyrite disease’’ texture (DIS-ccp) mainly formed in deeper levels [13, 14, 15], showing iron content of up to 3.1 wt. %. Chalcopyrite is associated with galena and sphalerite, and is also formed as inclusions in sphalerite and galena (Fig. 11e). Glena is mostly associated with sphalerite and chalcopyrite.

Sub-stage 3B is characterized by deposition of fine quartz; galena and sphalerite vein and veinlets associated with sulfosalts which cross cut the sulfides in the sub-stage 3A. Minerals such as zincian-tetrahedrite, argentinian-tetrahedrite, tetrahedrite, chalcostibite ($CuSbS_2$), seligmanite, tenantite and argentite are major inclusions in galena (Fig. 11f). Greenockite (Fig. 11g) and two phases of Pb-Zn-Cd solid solutions were detected by electron microprobe in shallower levels as inclusions in galena. This sub-stage has highest silver content in Glojeh veins (200 g/t), and content of Se in this silver bearing minerals is very low, probably reflects a relatively reduced environment consistent with intermediate sulfidation state [16].

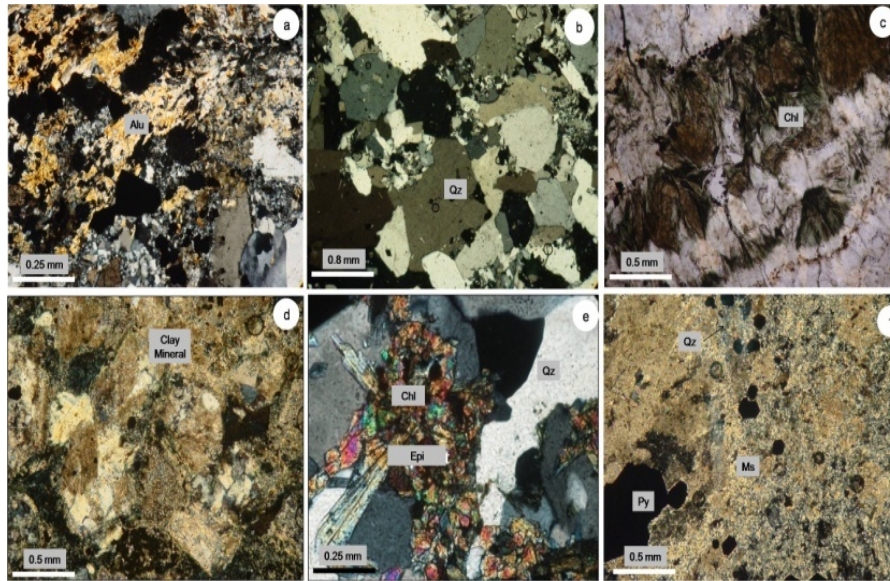


Fig. 8. Photomicrographs of alteration types related with North Glojeh vein mineralization: a) Subhedral alunitic mineralization in advanced argillic zone close to the veins and associated by mineralization in stage; b) Crustiform quartz in silicic zone; c) Argillic zone rich in chlorite associated by Pb-Zn-Ag mineralization in stage 3B; d) argillic zone; e) Propylitic zone consist of chlorite, epidote, albite and calcite and f) Quartz, pyrite, fine grain muscovite and minor calcite in sericitic alteration. Abbreviations: (Qz) quartz, (Pl) plagioclase, (Py) pyrite, (Mus) muscovite, (Alu) alunitic and (Chl) chlorite.

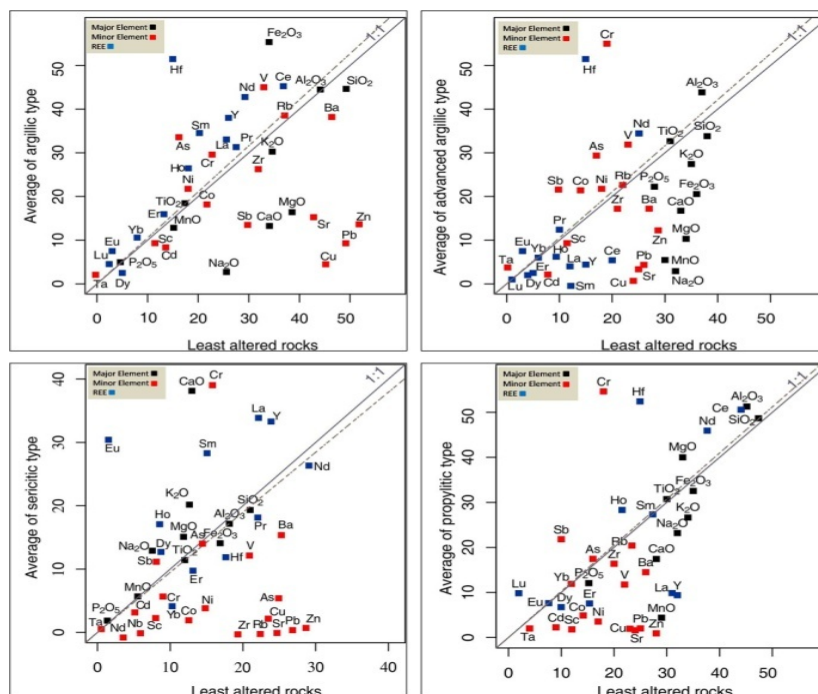


Fig. 9. Isocon diagrams for alteration zones calculated according to [12].

Table 1. Sample analyses from the North Glojeh veins. Major oxides were analyzed by XRF at the Kharazmi University (Iran), and other elements were analyzed by ICP-MS at ACME Labs (Canada).

	G27	G28	G29	G30	G31	G32	G33	G34	G35	G36	G37	G38	G40	G41
sample	Va-gr-19	Go-gr-12	Gl1-HR-09	Va-gr-15	Go-gr-10	Go-gr-11	Go-Dy-07	Go-Dy-08	Gl1-20	Gl1-20-01	GlS-Ts-H15	GlS-Ts-H15b	Go-Dy-08	GlS-BH3-H14
SiO2 (wt%)	68.47	68.70	70.47	70.47	70.75	60.92	65.57	62.09	69.76	55.24	55.62	50.41	52.05	52.15
TiO2	0.55	0.57	0.29	0.45	0.45	0.93	0.73	0.77	0.32	0.17	0.79	1.02	0.98	0.95
Al2O3	14.30	14.28	11.60	12.50	11.55	14.40	14.68	14.80	10.80	7.00	15.30	14.20	16.00	16.15
Fe2O3 (tot)	2.86	3.20	3.00	3.10	4.00	7.50	5.10	5.60	3.90	28.00	7.50	9.50	8.30	10.20
MnO	0.05	0.08	0.08	0.05	0.10	0.24	0.18	0.24	0.14	0.06	0.49	0.48	0.24	0.62
MgO	0.78	0.83	0.43	0.35	0.75	2.13	0.99	1.44	0.76	0.27	2.15	5.15	2.10	4.90
CaO	2.00	1.60	4.40	1.80	1.95	5.40	1.60	4.45	0.28	3.50	8.60	8.68	5.80	0.70
Na2O	3.80	3.40	1.13	3.40	2.80	3.82	3.50	3.60	0.25	0.19	0.06	1.21	4.00	0.16
K2O	5.12	5.10	3.80	5.45	5.08	3.80	4.25	4.00	6.35	3.10	3.15	4.10	3.80	4.20
P2O5	0.14	0.13	0.07	0.06	0.12	0.06	0.24	0.32	0.04	0.06	0.26	0.30	0.32	0.29
LOI	1.17	1.20	2.20	0.50	2.09	0.80	2.16	1.25	5.60	1.41	5.30	3.22	0.40	9.60
Total	99.17	99.09	98.47	98.13	99.00	100.00	99.00	98.56	98.60	99.00	98.92	98.27	99.99	99.92
Ppm														
Au	<0.1	<0.1	0.9	<0.1	<0.1	<0.1	<0.1	<0.1	0.1	1.0	<0.1	<0.1	<0.1	<0.1
Ag	<20.0	<20.0	8807.0	69.0	130.0	37.0	219.0	70.0	4233.0	5175.0	543.0	135.0	57.0	2931.0
As	7.70	4.0	54.0	9.6	3.4	5.6	36.1	7.8	36.3	448.8	144.6	74.5	5.0	24.4
Ba	424.0	368.0	544.0	201.0	470.0	689.0	925.0	739.0	778.0	590.0	319.0	1033.0	724.0	1143.0
Bi	<0.04	<0.04	13.9	0.1	0.05	<0.04	0.1	<0.04	1.0	8.7	0.2	0.1	<0.04	0.7
Co	4.5	5.7	13.5	2.7	4.7	19.7	8.5	10.1	10.7	12.4	25.7	29.0	19.9	35.2
Cr	37.0	41.0	55.0	54.0	45.0	21.0	24.0	40.0	55.0	38.0	53.0	88.0	28.0	63.0
Ni	3.0	3.1	2.5	3.9	2.8	8.6	2.8	3.5	2.1	1.8	21.8	36.2	9.7	30.3
Nb	41.0	42.8	7.2	47.8	31.2	12.6	17.8	17.1	17.3	7.2	8.6	12.2	12.1	9.0
Rb	248.3	288.7	124.7	320.5	266.5	62.1	209.3	109.3	202.1	106.3	153.3	108.8	95.7	136.2
Sb	0.6	0.8	53.7	2.0	0.6	1.2	5.8	0.9	15.5	49.8	18.9	6.3	1.4	11.9
Sc	5.7	6.2	4.1	3.6	4.7	18.1	9.6	9.2	2.4	6.4	24.2	28.1	23.7	33.1
Sn	2.2	2.9	0.7	2.4	1.6	1.6	2.7	2.4	2.8	1.0	1.3	1.6	1.7	1.1
Sr	299.0	258.0	76.0	117.0	213.0	424.0	302.0	398.0	52.0	44.0	83.0	221.0	468.0	96.0
Th	33.3	40.2	4.2	45.5	31.7	4.9	9.0	7.3	10.7	3.2	4.9	6.4	8.6	4.1
Zr	17.9	12.9	43.6	7.8	12.2	12.0	194.6	13.5	82.7	27.8	85.0	84.6	9.3	66.2

Be	5.0	5.0	6.0	6.0	4.0	2.0	1.0	3.0	2.0	8.0	2.0	2.0	2.0	2.0
U	4.5	7.0	1.8	9.2	6.8	1.0	2.5	1.9	3.0	1.0	2.4	1.9	1.7	1.7
Zn	32.0	40.0	3855.0	47.8	48.2	97.5	122.0	108.1	2968.6	3130.9	342.7	279.7	65.0	1558.1
Pb	23.0	23.8	1269.6	30.0	25.0	19.4	10.0	27.7	308.6	4156.2	733.7	216.3	19.1	68.3
V	30.0	39.0	37.0	12.0	32.0	176.0	75.0	102.0	21.0	49.0	221.0	224.0	187.0	276.0
Y	24.9	29.6	7.2	24.1	23.9	22.2	23.2	21.6	14.9	23.7	20.5	24.5	28.4	22.5
Cu	25.3	47.9	309.1	26.0	27.7	39.1	4.0	33.3	167.0	769.0	138.2	44.0	15.2	105.7
Mn	398.0	648.0	582.0	364.0	766.0	1836.0	1420.0	1859.0	1097.0	459.0	3791.0	3703.0	1879.0	4828.0
Mo	1.5	3.2	1.1	1.0	0.8	0.9	1.0	1.2	0.8	3.9	4.9	1.5	1.1	0.8
Cd	0.02	0.03	1.4	0.04	0.1	0.2	0.1	0.3	3.0	15.6	3.0	0.7	0.1	13.3
W	2.1	7.3	8.1	2.1	2.0	1.1	2.1	1.3	4.2	54.9	2.8	2.1	0.7	1.3
La	45.0	49.7	14.0	47.8	40.0	17.4	27.6	23.7	18.9	19.8	24.0	31.1	26.5	20.3
Ce	88.0	98.7	28.0	93.5	76.7	39.1	58.6	50.3	39.3	32.9	42.8	62.2	55.8	44.3
Nd	34.1	38.4	11.7	32.9	28.4	19.9	26.1	22.8	16.6	19.1	21.3	30.2	26.4	24.9
Sm	6.2	7.3	2.1	5.6	5.2	4.7	5.4	4.6	3.6	4.1	4.4	6.2	5.3	5.5
Eu	0.9	0.8	0.4	0.6	0.6	1.1	1.1	1.1	0.6	0.9	1.0	1.4	1.4	1.2
Hf	0.7	0.5	1.3	0.4	0.5	0.5	5.2	0.4	2.6	0.8	2.5	2.8	0.4	2.1
Lu	0.4	0.5	0.1	0.4	0.4	0.4	0.4	0.4	0.3	0.2	0.2	0.3	0.4	0.2
Pr	9.7	10.8	3.3	9.5	8.2	4.8	6.7	6.0	4.6	4.9	5.1	7.5	6.4	5.9
Gd	5.1	5.6	1.4	4.5	4.5	4.8	4.7	4.4	3.0	4.9	4.7	5.5	5.2	4.8
Yb	3.0	3.3	1.0	3.0	2.8	2.4	2.7	2.2	1.8	1.7	1.9	2.3	2.9	2.0
Er	2.9	3.5	0.8	2.8	2.6	2.6	2.6	2.4	1.7	2.2	2.2	2.5	3.0	2.3
Tb	0.8	1.0	0.2	0.8	0.8	0.8	0.7	0.7	0.5	0.8	0.7	0.9	0.9	0.7
Dy	4.6	5.7	1.2	4.4	4.5	4.4	4.3	4.5	3.0	5.0	3.0	1.0	2.0	3.0
Ho	0.9	1.1	0.2	1.0	0.9	0.9	0.9	0.9	0.6	4.6	3.5	4.5	4.8	4.0
Tm	0.4	0.5	0.1	0.4	0.4	0.4	0.4	0.3	0.3	0.3	0.3	0.3	0.5	0.3
Li	20.1	10.8	58.9	26.5	14.9	20.6	57.8	11.8	33.8	55.6	33.1	40.2	18.6	35.0
Ta	2.6	2.9	0.5	3.2	2.1	0.8	1.2	1.1	1.2	0.5	0.5	0.8	0.9	0.6
Cs	8.7	12.3	3.9	10.3	6.4	3.3	4.4	2.4	4.1	9.6	10.9	8.6	3.4	6.7

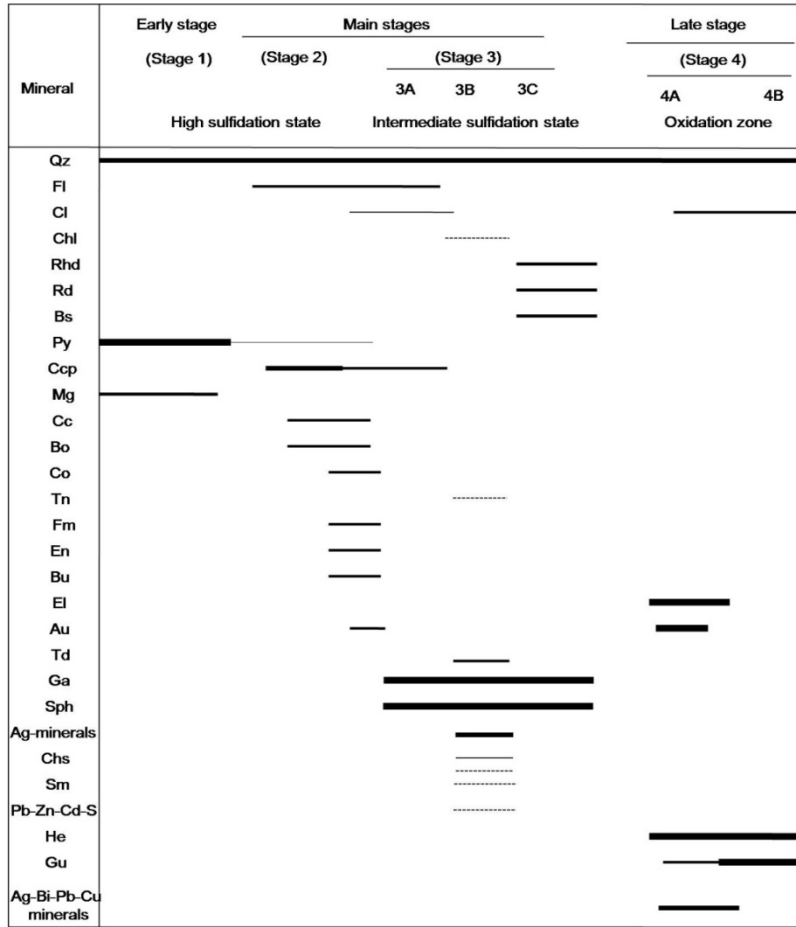


Fig. 10. Paragenetic sequence of ore and gangue minerals of North Glojeh mineralization. Abbreviations: (Bo) bornite, (Cc) chalcocite, (Co) covellit, (Bu) bournonite, (Fm) famatinite, (Qz) quartz, (Ccp) chalcopyrite, (Py) pyrite, (Sph) sphalerite, (Ga) galena, (Fl) fluorite, (Cl) chlorite, (Hm) hematite, (Au) native gold, (Ar) argentite, (Ag) native silver, (Zn-Td) zincian-tetrahedrite, (Gk) Greenockite, (Pb-Zn-Cd-S) unnamed mineral, (Ma) marrite, (Gb) galenobismuthite, (Pl) polybasite, (Me) meneghinite, (Bi) bismotinite, (Mt) matildite, (Ak) aikinite, (El) electrum and Tenantite (Tn).

A submicrometric intergrowth of native silver on argentite was detected during electron-microprobe analyses. Quartz and chlorite are main gangue minerals in this sub-stage. Sub-stage 3C is characterized by the deposition of tiny veinlet of galena, sphalerite, Mn-bearing silicate and carbonates in association with quartz.

Galena and sphalerite are major sulfides in this sub-stage. Mn-bearing silicates are rhodonite (MnSiO₃) and bustamite (CaMnSiO₃) and Mn-carbonates, rhodocrosite (Mn [CO₃]₂) in associated with quartz and calcite are main gangue minerals. Stage 4 is characterized by oxidation and deposition of precious metals in quartz vein in association with dark hematite-goethite as vugs infilling (open space filling texture) and subdivided into two sub-stages. Sub-stage 4A is characterized by a wide variety of precious and sulfosalt minerals, which don't show distinct paragenetic sequence. By decreasing

abundance, these are: matildite, galenobismuthinite, Au–Ag alloy, native silver, native gold, meneghinite, polybasite, marriite and aikinite (Figs. 11h, k). These minerals are abundant as inclusions in hematite. Sub-stage 4B is characterized by deposition of hematite and goethite in upper levels without any mineral inclusions. The relative volumes of hematite–goethite, and their Au and Ag contents, confirm that hematite–goethite precipitation controlled the main Au-fixing event in the North Glojeh deposit in its ultimate form. However, the Au/Ag ratio for this assemblage, ~0.50, is almost three times more than of the average, ~0.16. This implies that Stage 4 oxidation involved remobilization and reprecipitation of metals such as Au–Ag–Bi–Pb, which originally introduced in Stage 2 and 3. Au–Ag alloy occurs as inclusions in hematite, with crystal size of 10 up to 60 micron. Native gold (up to 15 micron) occurs as free grain in grey quartz and as inclusions in hematite. The bismuth minerals in North Glojeh are represented by matildite, native bismuth, galenobismuthinite and aikinite. Polybasite is also a silver-carrier mineral in North Glojeh mineralization. It occurs with meneghinite as small (up to 4 μm) inclusions in hematite. Quartz, calcite and chlorite are major gangue in stage 4.

5. Geochemistry

The data used in this study is in units of parts per million (ppm) for Au, Ag, As and Sb and in percent (%) for Pb, Zn, and Cu. Table 2, summarizes the basic statistics of the precious and base metal assay data. The average values for Au concentrations of the North Glojeh veins is 2.1 ppm. The average Pb+Zn values for veins is 2.0 percent. The Cu values are generally low and erratic and occur at deeper levels. The average Cu values in the two veins that have copper assays in the data base, range from 0.00 to 0.9 percent. Correlation matrices were calculated for the assay data of every vein separately (Table 3). The calculations show that Zn and Pb have the highest correlation (0.9). Also Pb have the highest correlation with Ag (0.9). The high correlation between Ag and Pb supports the observation that Ag sulfosalts in Galena (stage 3B). The correlation between Ag and Cu is low (0.4), that suggests silver and copper do not coexist. The correlation between Au and Ag (0.7) is high, as well as the correlation between Au and As (0.6), which suggests that the distribution of Au within the vein match exactly either the distribution of Ag and As. In order to illustrate the distribution of the elements in the veins, we prepared longitudinal sections for the two veins using the chemical assays and their corresponding “x” (easting) and “y” (elevation) coordinates. Longitudinal sections of Ag/Pb, Au/Ag, Pb+Zn and Cu+As equivalent (eq.) were plotted for the North Glojeh veins (Fig. 12). The longitudinal sections of the veins show that Pb, Zn and especially Cu+As are concentrated at depth and that the precious metals occur at shallow elevations, above the base metals zones. Additionally, the ore bands defined by Ag/Pb ratios value occur between the base metals zone and a band defined by high Au/Ag ratios at shallower levels.

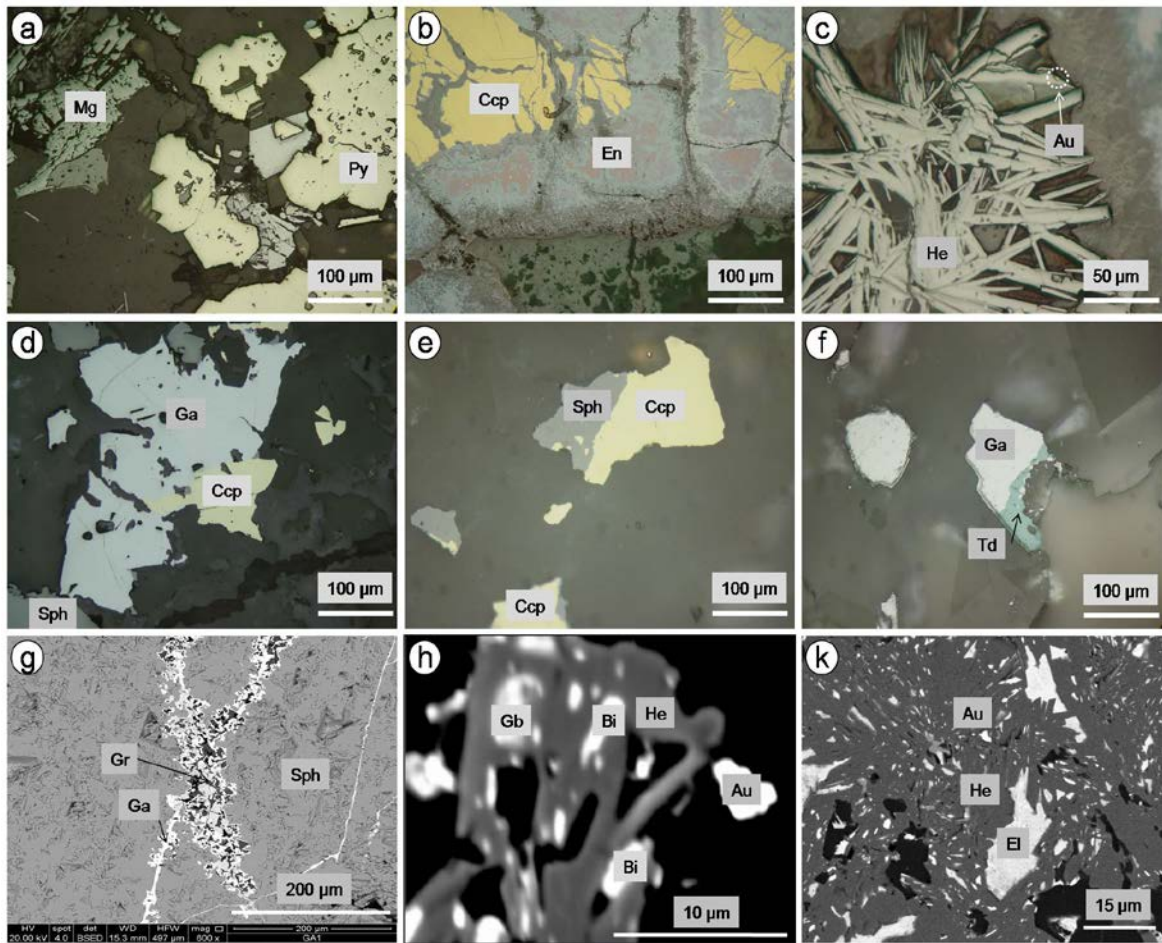


Fig. 11. Reflected light, SEM and EPMA photomicrographs showing replacement textures and ore minerals relationships: a) Pyrite replaced by chalcopyrite, sphalerite and galena; b). Cu sulfide minerals in stages 2; c) native gold in stage 2; d and e) Sphalerite and galena in sub-stage 3A; f) Tetrahedrite inclusion in galena (sub-stage 3B); g) greenockite (Gr) as inclusion in galena associated with sphalerite in sub-stage 3B and h and k) gold and Bi bearing mineral associated by hematite in sub-stage 4A. For abbreviation see Fig. 10.

Table 2. Summary table showing basic statistics for the North Glojeh veins

		Minimum	Maximum	Mean	Std. Deviation
N Glojeh (N=320)	Au (ppm)	0.03	40.5	2.1	165.97
	Ag (ppm)	0.32	420	18	145.8
	As (ppm)	9.7	1719	215	301.2
	Sb (ppm)	0.9	186	20	270.2
	Cu (%)	00	0.9	0.05	2000.12
	Pb (%)	00	5	0.7	1958.03
	Zn (%)	0.1	13	1.3	2000.1

Table 3. Correlation matrices for North Glojeh veins.

N Glojeh								
	Au	Ag	Pb	Zn	Cu	As	Sb	Cd
Au	1.0							
Ag	0.7	1.0						
Pb	0.4	0.9	1.0					
Zn	0.3	0.5	0.9	1.0				
Cu	0.4	0.4	0.5	0.3	1.0			
As	0.6	0.3	0.5	0.4	0.7	1.0		
Sb	0.5	0.6	0.5	0.4	0.3	0.4	1.0	
Cd	0.3	0.6	0.5	0.8	0.0	0.1	0.0	1.0

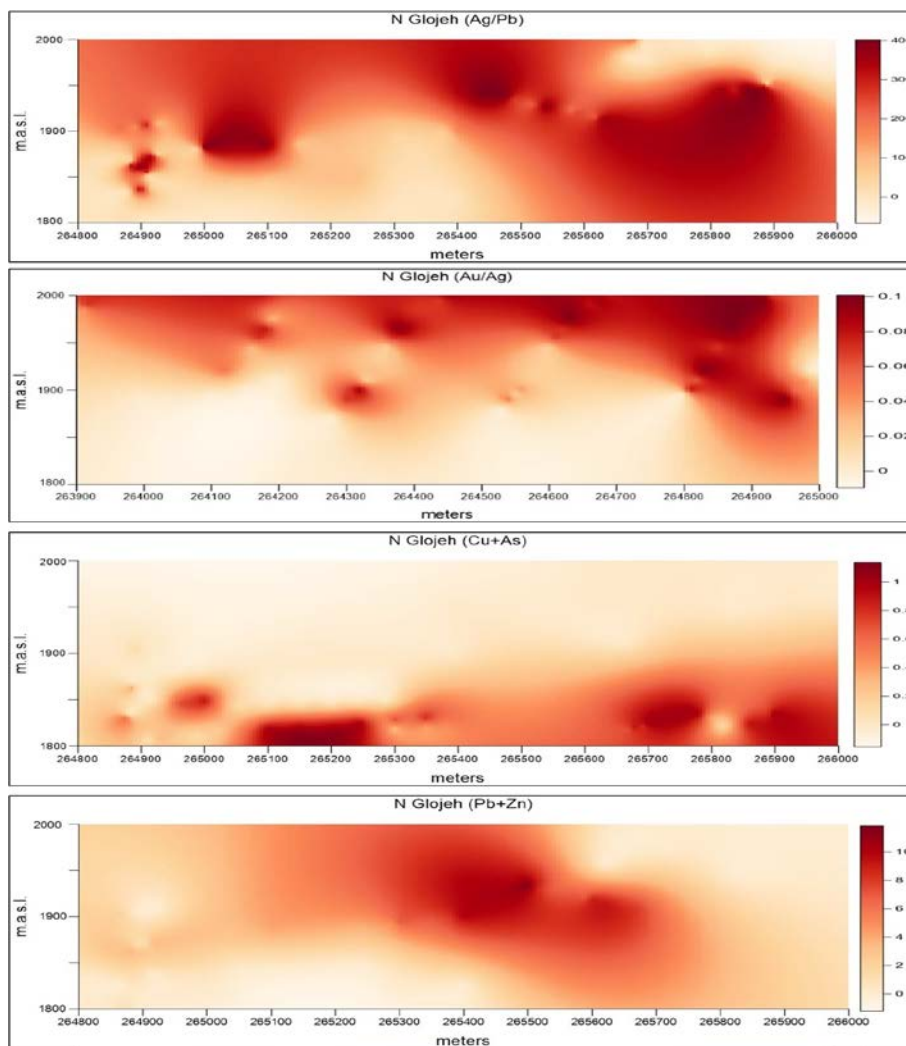


Fig. 12. Longitudinal sections of North Glojeh veins. Ag/Pb ratios showing the distribution of silver with respect to lead; Au/Ag ratios showing the distribution of gold with respect to silver; Cu+As and Pb+Zn. Elevation in meters above sea level (m.a.s.l.) and distance is in meters, the numbers represent the east coordinate in UTM.

6. Discussion

6.1. Geochemical Zoning

Variations in metal concentrations and metal ratios at the scale of individual veins in vertical longitudinal sections in North Glojeh occur. These variations are evidence of geochemical zoning. The longitudinal sections show clearly that Ag/Pb occurs at higher elevations and associated with base metals, which is supported by the observation that sub-stage 3B occur generally above the zone rich in base metals (sub-stage 3A). The base metals occur at the deepest levels, whereas gold and especially Au/Ag ratios seems to occur in shallower levels. This observation contradicts the typical zoning pattern caused by boiling in epithermal veins, where base metals occur at depth, silver at intermediate depth and gold at shallow depth [17, 18, 19, 20]. In the Purisima-Colon vein system, Pachuca, Mexico, the base metals are concentrated at depth, and there is an intermediate-depth zone with high silver grades overlapping the base metals zone [21].

6.2. North Glojeh as an epithermal deposit

North Glojeh veins share a common paragenesis including an early, massive pyrite and magnetite stage; a main stage contains Cu-Sb-As-Fe-S minerals and base metal with silver minerals; and late precious metals. The stage 1 and 2 mineralization is more akin to the high-sulfidation type, with alunite alteration assemblage and existence high sulfide minerals such as enargite and covellite and likely of magmatic derivation [22]. On the other hand, mineralization in stage 3 characterized by abundant base metal and silver associated manganese rich mineral and argillic alteration. Stage 3 could be compared with the intermediate-sulfidation type [23]. FS2 calculated for stage 3 (using Fe in sphalerite) is consistent with intermediate sulfidation state (10-10.0–10-10.5). Our studies have demonstrated that Au and Ag were introduced during Stage 2 and 3 sulfide mineralization, and were subsequently remobilized during oxidation by relatively low-temperature fluids dominated by meteoric water in stage 4. North Glojeh veins may be summarized as a case of progressive shifting with time from magmatic-controlled hydrothermalism (stage 1 and 2) toward meteoric-dominated hydrothermalism (precious metal deposition). Silver and base metal transport in the epithermal environment is dominated by chloride complexes [27, 28]. These complexes are more important for silver and base metal transport rather than for gold. In contrast, the Au (HS)₂- bisulfide complex is most important species for gold transportation in the epithermal environment [27], and thus gold transport is not affected by salinity in the same way as silver and base metals. Boiling and mixing are the two principal physical processes affecting mineral deposition in hydrothermal systems [28]. Boiling occurs in the up flow of most high permeability systems, whereas linear thermal profiles are common on the margins (due to mixing or low permeability; [29]). The relationship between fluid inclusion Th and Tmice data from the North Glojeh veins [30] clearly shows a trend of boiling, mixing and dilution. Boiling has been documented in other epithermal systems as well, and has been empirically invoked as the principal process controlling metal deposition [31].

7. Conclusion

- Ore deposition was related to the development of a high enthalpy geothermal system in THMP, and related to Eocene to Oligocene volcano-plutonism.
- The North Glojeh district is a classic example of silver-base metal epithermal mineralization in Iran, and is one of the principal orebodies in the THMP.
- The mineralization process occurred in four stages. During stage 1 and 2, magmatic and hot acid sulfur- rich fluids deposited massive sulfides (pyrite, Cu sulfides). During stage 3, base metal sulfides, then precious metal mineralization (stage 4).
- The North Glojeh deposit is a typical epithermal deposit, with features of either high-sulfidation (stage 1 and 2) associated with advanced argilic alteration, or intermediate-sulfidation (stage 3) types of epithermal deposits associated with argilic alteration (chlorite zone). Stage 4 also show features of low sulfidation type of epithermal ore deposits.
- Longitudinal sections of the veins show that the base metals are concentrated at depth and precious metals at shallow levels, which is in agreement with metal zoning in boiling systems.

8. References

- [1] JW. Hedenquist. AJr. Arribas. JT. Reynolds. "Evolution of an Intrusion-Centered Hydrothermal System: Far Southeast-Lepanto Porphyry and Epithermal Cu-Au Deposits, Philippines". *Economic Geology*, vol. 93, pp. 373–404, 1998.
- [2] F. Pirajno. RE. Ernst. AS. Borisenko. "Intraplate magmatism in Central Asia and China and associated metallogeny". *Ore Geology Reviews*, vol. 35, pp. 114-136, 2009.
- [3] S. Jankovic. "The Carpatho-Balkanides and adjacent area: a sector of the Tethyan Eurasian metallogenic belt". *Mineralium Deposita*, vol. 32, pp. 426–433, 1997.
- [4] ZM. Yang. ZQ. Hou. NC. White. ZS. Chang. ZQ. Li. YC. Song. "Geology of the post-collisional porphyry copper-molybdenum deposit at Qulong, Tibet". *Ore Geology Reviews*, vol. 36, pp. 133–159, 2009.
- [5] J. Stocklin. "Structural history and Tectonic of Iran". a review, *Am. Assoc. of Petroleum Geologists Bul.*, vol. 52, pp. 1229-1258, 1968.
- [6] J. Stocklin. "Possible ancient continental margins in Iran. In: CA. Burk. CL. Drake. (Eds.), *The Geology of Continental Margins*". *Springer, Berlin*, pp. 873–887, 1974.
- [7] H. Azizi. A. Jahangiri. "Cretaceous subduction-related volcanism in the Northern Sanandaj Sirjan zone, Iran". *Journal of Geodynamic*, vol. 45, pp. 178-190, 2008.
- [8] Geological Survey of Iran. "Geological map of Hashtjin". N 5664, 1995.

- [9] A. Peccerillo. and SR. Taylor. “Geochemistry of Eocene calc alkaline volcanic rocks from the Kastamonu area”. *Northern Turkey contribution of mineralogy of petrology*, vol 58, pp. 63-81, 1976.
- [10] D. Muller. NMS. Rock. DI. Groves. “Geochemical discrimination between shoshonitic and potassic volcanic rocks in different tectonic settings, a pilot study”. *Mineral. Petrol*, vol. 46, pp. 259–289, 1992.
- [11] JA. Pearce. “Trace element characteristics of lavas from destructive plate boundaries”. In, *Thorpe, R.S, Wiley, New York*, pp. 525–548, 1982.
- [12] JA. Grant. “The isocon diagram-A simple solution to Geresens equation for metasomatic alteration”. *Economic Geology*, vol 81, pp. 1976-1982, 1986.
- [13] PB. Barton. PM. Bethke. “Chalcopyrite disease in sphalerite: Pathology and epidemiology”. *American Mineralogy*, vol. 72, pp. 451–467, 1987.
- [14] K. Bente. T. Doring. “Solid-state diffusion in sphalerites: an experimental verification of the chalcopyrite disease”. *Eur. J. Mineral*, vol. 5, pp. 465-478, 1993.
- [15] K. Bente. T. Doring. “Experimental studies on the solid state diffusion of Cu and In in ZnS and on “disease”, DIS (Diffusion Induced Segregations), in sphalerite and their geological applications”. *Mineral Petrol*, vol. 53, pp. 285-305, 1995.
- [16] G. Simon. SE. Kesler. EJ. Essene. “Phase relations among selenides, sulfides, tellurides, and oxides: II. Applications to selenide- bearing ore deposits”. *Economic Geology*, vol. 92, pp. 468–484, 1997.
- [17] LJ. Buchanan. “Precious Metal Deposits Associated with Volcanic Environments in the Southwest: In Relations of Tectonics to Ore Deposits in the Southern Cordillera”. Eds. W.R. Dickson and W.D. Payne, *Geological Society of Arizona, Digest*, vol. 14, pp. 237–262, 1981.
- [18] SE. Drummond. H. Ohmoto. “Chemical evolution and mineral deposition in boiling hydrothermal systems”. *Economic Geology*, vol. 80, pp. 126–147, 1985.
- [19] JB. Gemmill. SF. Simmons. H. Zantop. “The Santo Niño Silver-Lead-Zinc Vein, Fresnillo District, Zacatecas, Mexico: Part I. Structure, Vein Stratigraphy, and Mineralogy”. *Economic Geology*, vol. 83, pp. 1597–1618, 1988.
- [20] L. Grancea. L. Bailey. J. Leroy. D. Banks. E. Marcoux. JP. Milési. M. Cuney. AS. André. D. Istvan. C. Fabre. “Fluid evolution in the Baia Mare epithermal gold/polymetallic district, Inner Carpathians, Romania”. *Mineralium Deposita*, vol. 37, pp. 630–647, 2002.
- [21] JE. Dreier. “The Environment of vein Formation and Ore Deposition in the Purisima-Colon Vein

System, Pachuca Real del Monte District, Hidalgo, Mexico”. *Economic Geology*, vol. 100, pp. 1325 – 1347, 2005.

[22] RH. Sillitoe. “Epithermal models: Genetic types, geometrical controls and shallow features”. *Geological Association of Canada Special Paper*, vol. 40, pp. 403–417, 1993a.

[23] MT. Einaudi. JW. Hedenquist. EE. Inan. “Sulfidation state of fluids in active and extinct hydrothermal systems, Transitions from porphyry to epithermal environments. In: Simmons. SF. Graham. I. (eds) Volcanic, geothermal, and ore-forming fluids, rulers and witnesses of processes within the earth”. *Society of Economic Geologists Special Publication*. vol. 10, pp. 285–313, 2003.

[24] J. Vallance. M. Boiron. M. Cathelineau. S. Fourcade. M. Varlet. C. Marignac. “The granite hosted gold deposit of Moulin de Cheni (Saint-Yrieix district, Massif Central, France): petrographic, structural, fluid inclusion and oxygen isotope constraints”. *Mineralium Deposita*, vol. 39, pp. 265-281, 2004.

[25] TM. Seward. HL. Barnes. “Metal transport by hydrothermal ore fluids, in Barnes, HL. ed. *Geochemistry of hydrothermal ore deposits*”. *New York, John Wiley and Sons*, pp. 435–486, 1997.

[26] G. Palyanaova. “Physicochemistry modeling of the coupled behavior of gold and silver in hydrothermal processes, gold fineness, Au/Ag ratios and their possible implications”. *Chemical Geology*, vol. 255, pp. 399-413, 2008.

[27] LG. Benning. TM. Seward. “Hydrosulfide complexing of Au in hydrothermal solutions from 150 to 400 °C and 500 to 1500 bars”. *Geochimica, Cosmochimica Acta*, vol. 60, pp. 1849–1871, 1996.

[28] WF. Giggenbach. MK. Stewart. “Processes controlling the isotopic composition of steam and water discharges from steam vents and steam-heated pools in geothermal areas”. *Geothermics*, vol. 11, pp. 71–80, 1982.

[29] JW. Hedenquist. E. Izawa. A. Arribas. NC. White. “Epithermal Gold Deposits: Styles, Characteristics and Exploration.” *Resource Geology Special Publication, Society of Resource Geology*, N. 1, p. 18, 1996.

[30] M. Ghasemi Siani. B. Mehrabi. H. Azizi. “Mineralogy, fluid inclusions and alteration of epithermal gold veins in Glojeh district, Zanjan”. *presented at the 1nd Int. Conf. Geoscience*, Tehran, Iran, 2014.

[31] D. Jr. Smith. TA. Albinson. FJ. Sawkins. “Geologic and fluid inclusion studies of the Tayoltita silver-gold vein deposit, Durango, Mexico.” *Economic Geology*, vol. 77, pp.1120–1145, 1982.